Chapter 4

Choice of precursor for synthesis of CuMnOx catalysts

4. General

Many methods have been established to prepare the CuMnOx catalysts, including co-precipitation, supercritical anti-solvent precipitation, ultrasonic aerosol pyrolysis, sol–gel and reduction methods. Among these methods, the conventional co-precipitation method can be used to produce CuMnOx catalysts with high activity [Cai *et al.,* 2012]. In this chapter, we have to investigate the choice of precursor and following calcination strategy on the catalytic performance of CuMnOx catalysts for CO oxidation. It is well-known that the various precursors used in the preparation of catalyst have a great influence on the activity of resulting catalysts [Jones *et al.,* 2008]. Thus, the state of precursor varies depending on the types of chemicals used, which result in the development of calcined catalysts with different crystalline phases and different catalytic performance [Irawan *et al.,* 2015]. The high activity is due to the formation of Cu-Mn spinel $CuMn_2O_4$ formed during co-precipitation process. The redox reaction has been proposed to explain the CuMnOx catalyst activity, i.e. an electron transfer between copper and manganese cations within the spinel lattice [Marinoiu *et al.,* 2014; Hu *et al.,* 2000]. It seems reasonable to conclude that the phase structure of CuMnOx catalysts has a significant influence on the activity of CO oxidation. The occurrence of individual phases and their quantitative proportions depend upon the temperature, pH and concentrations of the reactant solutions [Gardner and Hoflund 1991; Liu *et al.,* 2016].

The performance of the catalysts very much depends upon the calcination conditions of the precursors and the subsequent pretreatment of the catalysts [Mokhtar *et al.,* 2010; Marino *et al.,* 2005]. The high-temperature calcination causes sintering of the active crystallites with a subsequent loss of surface area and then adversely affects on the

performance of the catalyst [Choi *et al.,* 2016]. Therefore, to minimize the above mentioned drawbacks of two steps of calcination and pretreatment, a newer route of single step thermal treatment of the precursors in a reactive CO–air mixture at a low temperature has been recently suggested by the authors for preparing highly active catalysts by passing the separate pretreatment step [Prasad and Singh 2013]. Such single step thermal treatment of the precursor is called reactive calcination (RC) method. It is postulated that during the RC method parallel to diverse phenomena of CO oxidation and precursor decomposition, cause a synergistic effect in the formation of oxygen-deficient catalyst surface at a low temperature.

The success of CuMnOx catalyst has prompted a big deal of fundamental work devoted to clarifying the role played by each component and the nature of active sites. The activity of CuMnOx catalyst is also depending upon the structure and the preparation route [Larsson and Andersson 2000; Cole *et al.,* 2010]. Recently, Tang et al. have prepared the nano-crystalline CuMnOx catalysts using the supercritical anti-solvent precipitation method and found them to be more than twice as active as the conventionally prepared Hopcalite catalysts for CO oxidation [Tang *et al.,* 2011]. They can be attributed the high catalytic activity to the nano-crystalline and homogeneous nature of the synthesized CuMnOx catalyst [Hoshyar *et al.,* 2015]. The presence of MnO_2 is likely to assist the reduction of CuO, involving coordination between CuO and MnO_2, the MnO_2 acting as an oxygen donor and CuO acting as an oxygen acceptor [He *et al.,* 2017]. Previous work demonstrated that the presence of Cu^{2+} and Mn^{3+} is essential for the high catalytic activity of CuMnOx catalyst. In the present study, the different types of precursors have been used in order to change the crystalline phase of the catalysts for maximizing CO oxidation.

4.1 Experimental

4.1.1 Catalyst preparation

The CuMnOx catalysts were prepared by the co-precipitation method following the procedure described by Njagi *et al.,* 2010. All the chemicals used for the preparation of catalysts were of analytical grade. A solution of Mn-Acetate ($Mn(CH_3COO)_2.4H_2O$) or Mn-Nitrate ($Mn(NO_3)_2.4H_2O$) 5.50g in 20mL distilled water was added to 4.610gm of Cu-Acetate ($Cu(CH_3COO)_2.3H_2O$) or Cu-Nitrate ($Cu(NO_3)_2.3H_2O$) and stirred for 1h. The mixed solution was taken in the burette and added drop-wise to a solution of $KMnO_4$ (2.37gm in 20mL distilled water) under vigorous stirring conditions for co-precipitation purpose. The resultant precipitate was stirred continuously for 2h. The precipitate was filtered and washed several times with hot distilled water to remove all the anions. The cake thus obtained was dried at temperature 110^{o}C for 24h into an oven. The dried precursor thus obtained was divided into three parts for their calcination under three different strategies at 300^{o}C for 2h.

In the first strategy the precursor was calcined traditionally in a muffle furnace under stagnant air at 300°C for 2h. After calcination 4.72gm of catalyst was produced. The molar ratio of Cu and Mn in the final $CuMn_2$ catalyst was 1:2. The second strategy of calcination was under flowing air at a rate of 32.5 ml.min^{-1} at 300°C for 2h. The third strategy of calcination was carried out under reactive mixture of 4.5%CO in air calcination (RC) as follows: Reactive calcination of the precursor was carried out by the introduction of a low concentration of chemically reactive CO–Air mixture (4.5% CO) at a total flow rate of 32.5 ml.min^{-1} over the hot precursors. The temperature of the reactor bed was increased from room temperature to 160°C where CO conversion has started. This temperature was maintained for a defined period of time where the CO concentration has measured in the exit stream of the reactor at regular intervals until

100% CO conversion was achieved. After achieving total CO conversion the resultant catalyst was annealed for half an hour at the same temperature then the temperature was increased up to 300^{o}C and upheld for an hour followed by cooling to room temperature in the same environment. The nomenclature of the resulting catalysts thus formed was given by the suffixes '$_{SA}$', '$_{FA}$' and '$_{RC}$' denoting the calcination environment as stagnant air, flowing air or by RC respectively, as depicted in Table 4.1.

Table 4.1: Calcination strategy and nomenclature of catalysts

Precursor	**Calcination Strategy**	**Nomenclature**
$Mn(Ac)_2 + Cu(NO_3)_2$	Stagnant air calcination	$CuMn_{2SA1}$
$Mn(Ac)_2 + Cu(Ac)_2$		$CuMn_{2SA2}$
$Mn(NO_3)_2 + Cu(NO_3)_2$		$CuMn_{2SA3}$
$Mn(NO_3)_2 + Cu(Ac)_2$		$CuMn_{2SA4}$
$Mn(Ac)_2 + Cu(NO_3)_2$	Flowing air calcination	$CuMn_{2FA1}$
$Mn(Ac)_2 + Cu(Ac)_2$		$CuMn_{2FA2}$
$Mn(NO_3)_2 + Cu(NO_3)_2$		$CuMn_{2FA3}$
$Mn(NO_3)_2 + Cu(Ac)_2$		$CuMn_{2FA4}$
$Mn(Ac)_2 + Cu(NO_3)_2$	Reactive calcination	$CuMn_{2RC1}$
$Mn(Ac)_2 + Cu(Ac)_2$		$CuMn_{2RC2}$
$Mn(NO_3)_2 + Cu(NO_3)_2$		$CuMn_{2RC3}$
$Mn(NO_3)_2 + Cu(Ac)_2$		$CuMn_{2RC4}$

4.2 Catalyst Characterization

Characterization of all the CuMnOx catalysts prepared by reactive calcination method was done by the different techniques and discussed in the following sections. The characterization of the catalysts:

4.2.1 Morphological analysis

The Scanning Electron Micrographs (SEM) instrument was used for the microstructure analysis of the optimized Cu_1Mn_2 catalyst. The SEM micrographs (Figure 4.1) show clearly large differences in the microstructure and morphology of the $CuMn_{2RC}$ catalysts formed by different precursors. They all shows granular particles between 0.30 and 4µm calculated by "Image J software" with varying degree of agglomeration as mentioned in Table 4.2. As shown in SEM micrographs, the particles were comprised grains of more coarse, coarse, fine and finest sizes for $CuMn_{2RC4}$, $CuMn_{2RC3}$, $CuMn_{2RC2}$ and $CuMn_{2RC1}$ catalysts respectively. The SEM result was also in good agreement with XRD analysis. The average particle size of $CuMn_{2RC1,}$ $CuMn_{2RC2}$, $CuMn_{2RC3}$ and $CuMn_{2RC4}$ catalysts were 0.315µm, 0.816µm, 2.491µm and 3.825µm respectively. The particles of $CuMn_{2RC1}$ catalyst was least agglomerated, highly porous, higher surface area and uniformly distributed.

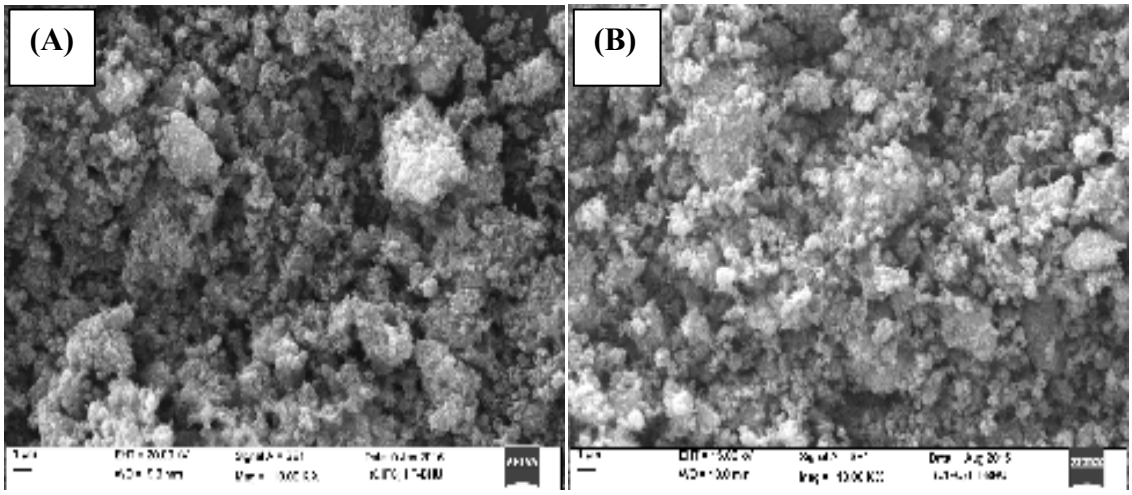

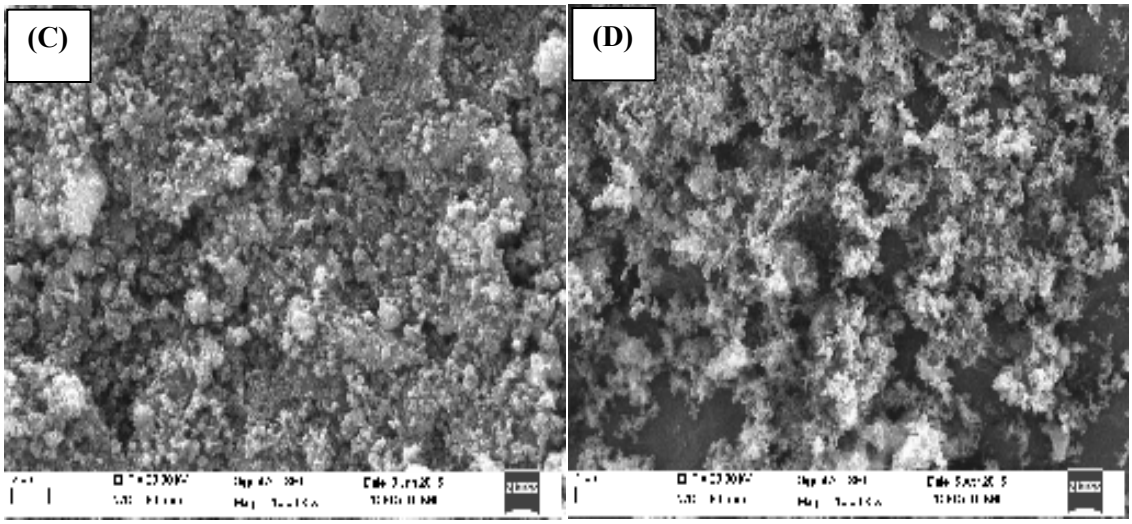

Figure 4.1: SEM image of (A) $CuMn_{2RC4}$, (B) $CuMn_{2RC3}$, (C) $CuMn_{2RC2}$ and (D) $CuMn_{2RC1}$

The choices of precursors in the CuMnOx catalysts lead to the change of surface distribution of Cu, Mn and O elements. Thus, the different precursors used in the preparation of CuMnOx (Cu_1Mn_2) catalyst in the present study significantly affect the particle size as well as the morphology of the resulting catalysts.

Table 4.2: Particle size of $CuMn_{2RC}$ catalysts

Precursor	Catalyst	Particle size (µm)
$Mn(Ac)_2 + Cu(NO_3)_2$	$CuMn_{2RC1}$	0.315
$Mn(Ac)_2 + Cu(Ac)_2$	$CuMn_{2RC2}$	0.816
$Mn(NO_3)_2 + Cu(NO_3)_2$	$CuMn_{2RC3}$	2.491
$Mn(NO_3)_2 + Cu(Ac)_2$	$CuMn_{2RC4}$	3.825

The synergetic effect of $CuMn_{2RC1}$ catalyst highly depends upon the catalyst composition and the nature of oxidized compound. All the catalysts have different morphologies, indicating that the types of precursors used in the preparation of catalyst have great influences on the catalyst performance. The mixing of $\{Mn(Ac)_2+Cu(NO_3)_2\}$ and precipitation by $KMnO_4$ solution was more efficient in production of finest particle size.

4.2.2 Elemental analysis

In order to verify the elemental percentage of CuMnOx catalysts by Scanning Electron Microscopy (SEM) with Energy Dispersive X-Ray analysis (SEM-EDX) technique was performed in a large scanning range by random for the samples of $CuMn_{2RC4}$, $CuMn_{2RC3}$, $CuMn_{2RC2}$ and $CuMn_{2RC1}$ catalysts. The elemental concentration distribution of the catalyst granules were determined by using Isis 300 software. The result of SEM-EDX analysis is shown in Table 4.3. It can be seen that all the catalyst samples were pure due to the existence of their relevant elemental peaks only. It was performed on different cross-sectioned marks of the Cu_1Mn_2 catalysts granules to determine the concentration of different elements located at different cross-section on the catalysts granular surfaces as shown in the Figure 4.2.

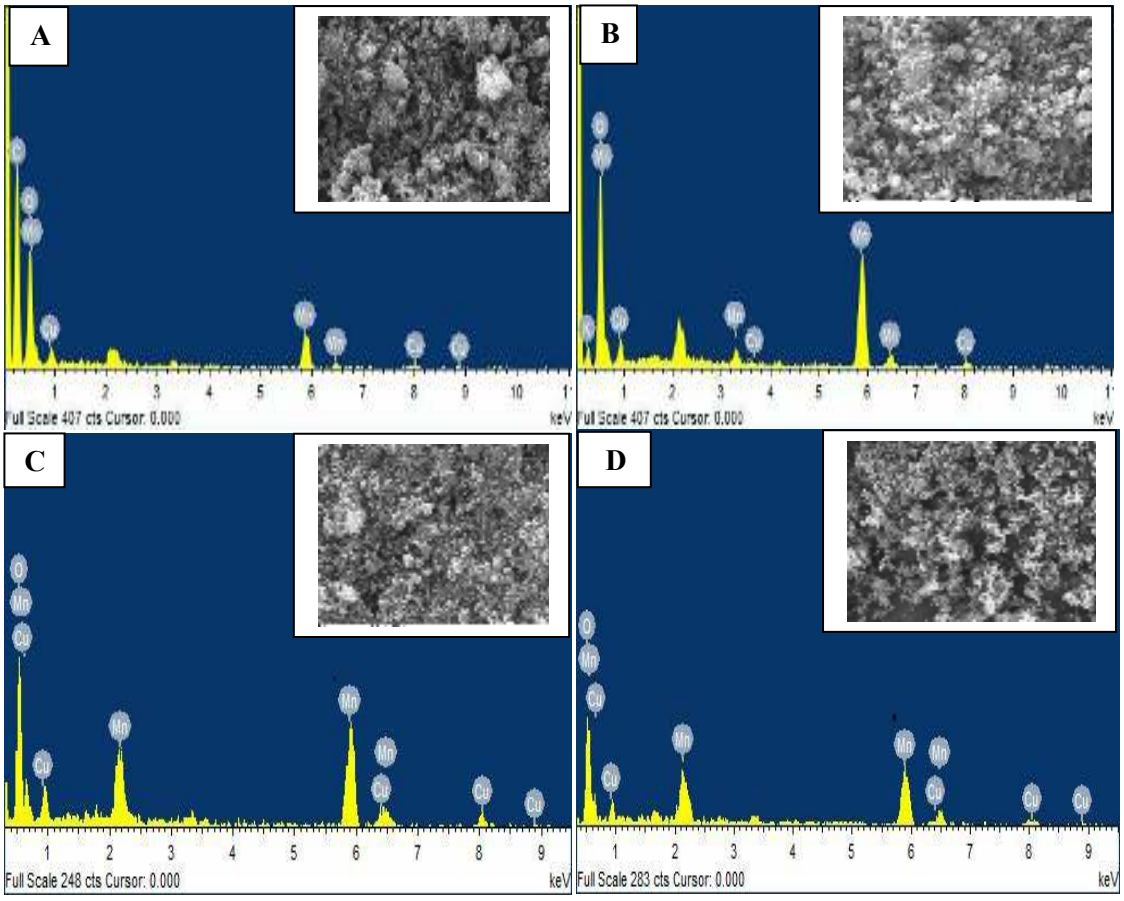

Figure 4.2: SEM-EDX image of (A) $CuMn_{2RC4}$, (B) $CuMn_{2RC3}$, (C) $CuMn_{2RC2}$ and (D) $CuMn_{2RC1}$

Table 4.3 represents the relative atomic abundance of Cu, Mn and O species present in the surface layers of CuMnOx catalysts. The presence of Cu, Mn and O on the surface of $CuMn_{2RC}$ catalysts can be clearly detected. The atomic ratio and weight ratio of Cu/Mn in the $CuMn_{2RC1}$ catalyst was approximately 0.558 and 0.567 respectively. The molar ratio of Cu/Mn in all the catalyst samples using co-precipitation method was approximately (0.512), and it was very close to the actual dosage of Cu and Mn present in the precursors.

Table 4.3: EDX analysis of $CuMn_{2RC}$ catalyst

Catalyst	Atomic ratio (%)				Weight ratio (%)			
	Cu	Mn	O	Cu/Mn	Cu	Mn	O	Cu/Mn
$CuMn_{2RC1}$	30.54	54.65	14.81	0.558	30.81	54.35	14.84	0.567
$CuMn_{2RC2}$	31.79	51.15	17.06	0.621	32.15	51.56	16.29	0.623
$CuMn_{2RC3}$	26.41	53.81	19.78	0.490	26.85	53.95	19.20	0.497
$CuMn_{2RC4}$	25.65	54.25	20.10	0.472	25.89	54.46	19.65	0.475

The abundant surface oxygen atoms of the $CuMn_{2RC}$ catalyst can react with the absorbed CO and thus lead to better catalytic activity in the Mars–van Krevelen type mechanism (MvK) which was frequently suggested for metal-oxides. The presence of oxygen deficiency in the $CuMn_{2RC1}$ catalyst was least, which makes the high density of active sites. It was clear from the Table 4.3 and Figure 4.2 that the atomic percentage and weight percentage of Mn was also higher as comparison of Cu and O. The choice of precursors leads to the change of surface distribution of Cu, Mn and O elements.

4.2.3 Phase identification and cell dimensions

The phase identification and cell dimensions of $CuMn_2$ catalysts prepared in reactive calcination conditions were done by the X-ray powder diffraction (XRD) technique. It

was carried out to recognize the crystallite size and coordinate dimensions present on the surface layer of $CuMn_2$ catalysts. XRD patterns of the Cu_1Mn_2 catalysts ($CuMn_{2RC1}$, $CuMn_{2RC2}$, $CuMn_{2RC3}$ and $CuMn_{2RC4}$) produced by reactive calcination of the various precursors are displayed in the Figure 4.3. XRD pattern of the $CuMn_{2RC1}$ catalyst has shown that the diffraction peak at 2θ of 36.96 corresponds to Face-centered cubic $Cu_1Mn_2O_4$ (PDF-70-0260 JCPDS file). The crystallite size of the catalyst determined by the Scherrer eq^n. (2.3.1) was 3.90 nm.

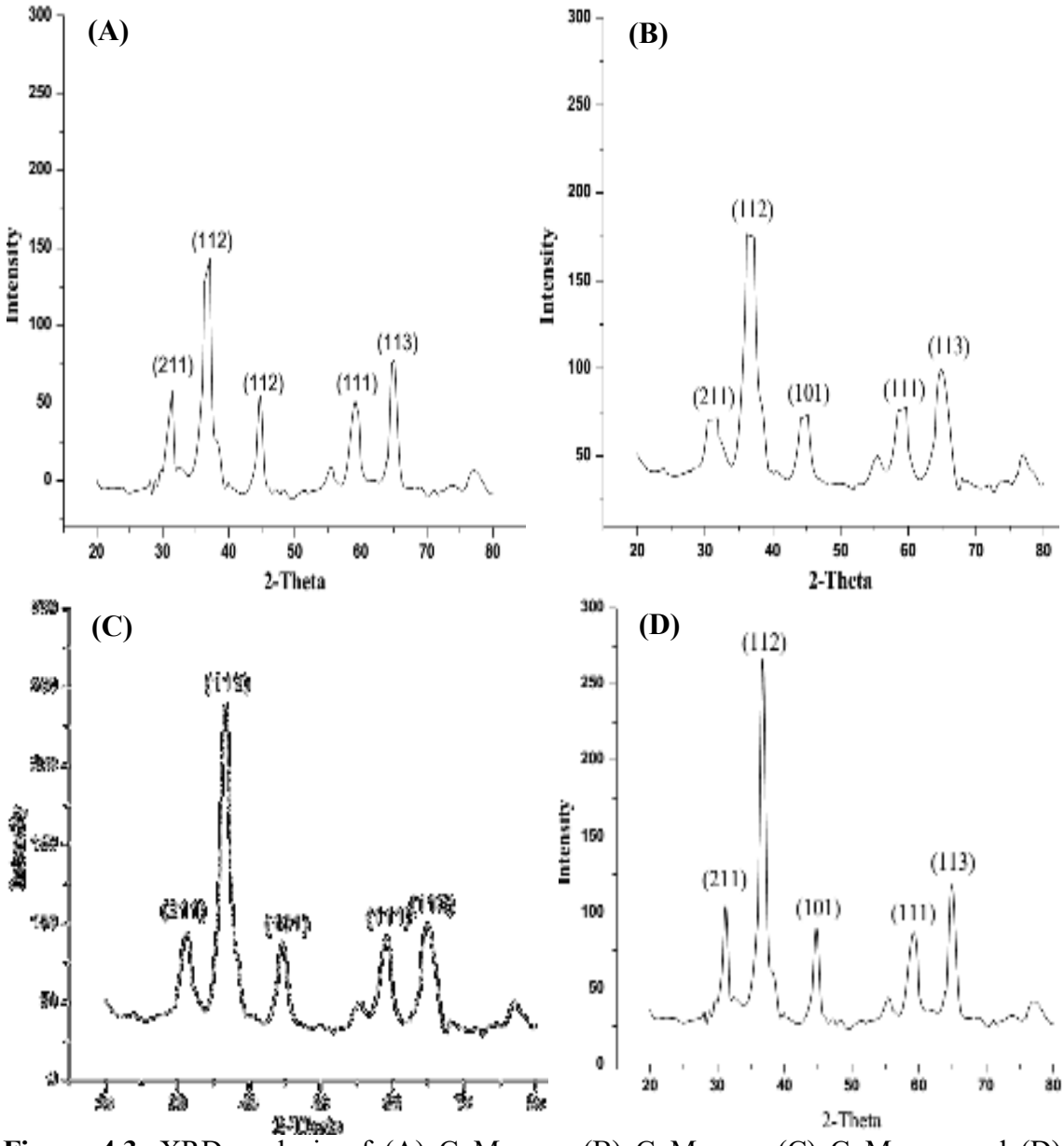

Figure 4.3: XRD analysis of (A) $CuMn_{2RC1}$, (B) $CuMn_{2RC2}$, (C) $CuMn_{2RC3}$ and (D) $CuMn_{2RC4}$

In reactive calcination, of $CuMn_{2RC2}$ catalyst has shown that the diffraction peak at 2θ of 36.60 corresponds to Face-centered cubic $Cu_1Mn_2O_4$ (PDF-70-0260 JCPDS file). The crystallite size of the catalyst was 4.22 nm. The XRD pattern of the $CuMn_{2RC3}$ catalyst has shown that the diffraction peak at 2θ of 37.23 corresponds to Face-centered cubic $Cu_1Mn_2O_4$ (PDF-70-0260 JCPDS file). The crystallite size of the catalyst was 5.61 nm. The XRD pattern of the $CuMn_{2RC4}$ catalyst has shown that the diffraction peak at 2θ of 38.43 corresponds to Face-centered cubic $Cu_1Mn_2O_4$ (PDF-70-0260 JCPDS file). The crystallite size of the catalyst was 7.90 nm. The structure, phase and crystallite size are given in Table 4.4.

Table 4.4: XRD analysis of $CuMn_{2RC}$ catalysts

Catalyst	Structure	Phase	Crystallite size
$CuMn_{2RC1}$	Face-centered cubic	$Cu_1Mn_2O_4$	3.90nm
$CuMn_{2RC2}$	Face-centered cubic	$Cu_1Mn_2O_4$	4.21nm
$CuMn_{2RC3}$	Face-centered cubic	$Cu_1Mn_2O_4$	5.61nm
$CuMn_{2RC4}$	Face-centered cubic	$Cu_1Mn_2O_4$	7.90nm

It was quite apparent from the Table 4.4 that the crystallite size of $CuMn_{2RC1}$ catalyst exhibited the smallest size (3.90nm) in comparison to $CuMn_{2RC2}$ (4.21nm), $CuMn_{2RC3}$ (5.61nm) and $CuMn_{2RC4}$ (7.90nm) catalysts. The order of crystallite size in descending order present in the catalyst samples obtained by RC conditions was as follows: $CuMn_{2RC4}$> $CuMn_{2RC3}$ > $CuMn_{2RC2}$> $CuMn_{2RC1.}$ The table and figure, confirmed that the particles present in $CuMn_{2RC1}$ catalyst was most crystalline form, and producing narrow size high-intensity diffraction peaks; as compared to other catalysts.

4.2.4 Identification of materials present in a catalyst

The identification of the functional group present in the catalyst surface was done by the Fourier transform infrared spectroscopy (FTIR) analysis. The different peaks show the various types of chemical groups present in the catalysts. The FTIR transmission spectrum of $CuMn_{2RC1}$, $CuMn_{2RC2}$, $CuMn_{2RC3}$ and $CuMn_{2RC4}$ catalysts prepared by reactive calcination (RC) condition is shown in Figure 4.4. In $CuMn_{2RC1}$ catalyst at the transmittance conditions (Figure 4.4A), there are total three peaks obtained, the IR band 1640cm^{-1} showed the presence of MnO_2 group, -OH group is showed at 3490cm^{-1} and wave number 1180cm^{-1} is showed CuO group [Cai *et al.,* 2012].

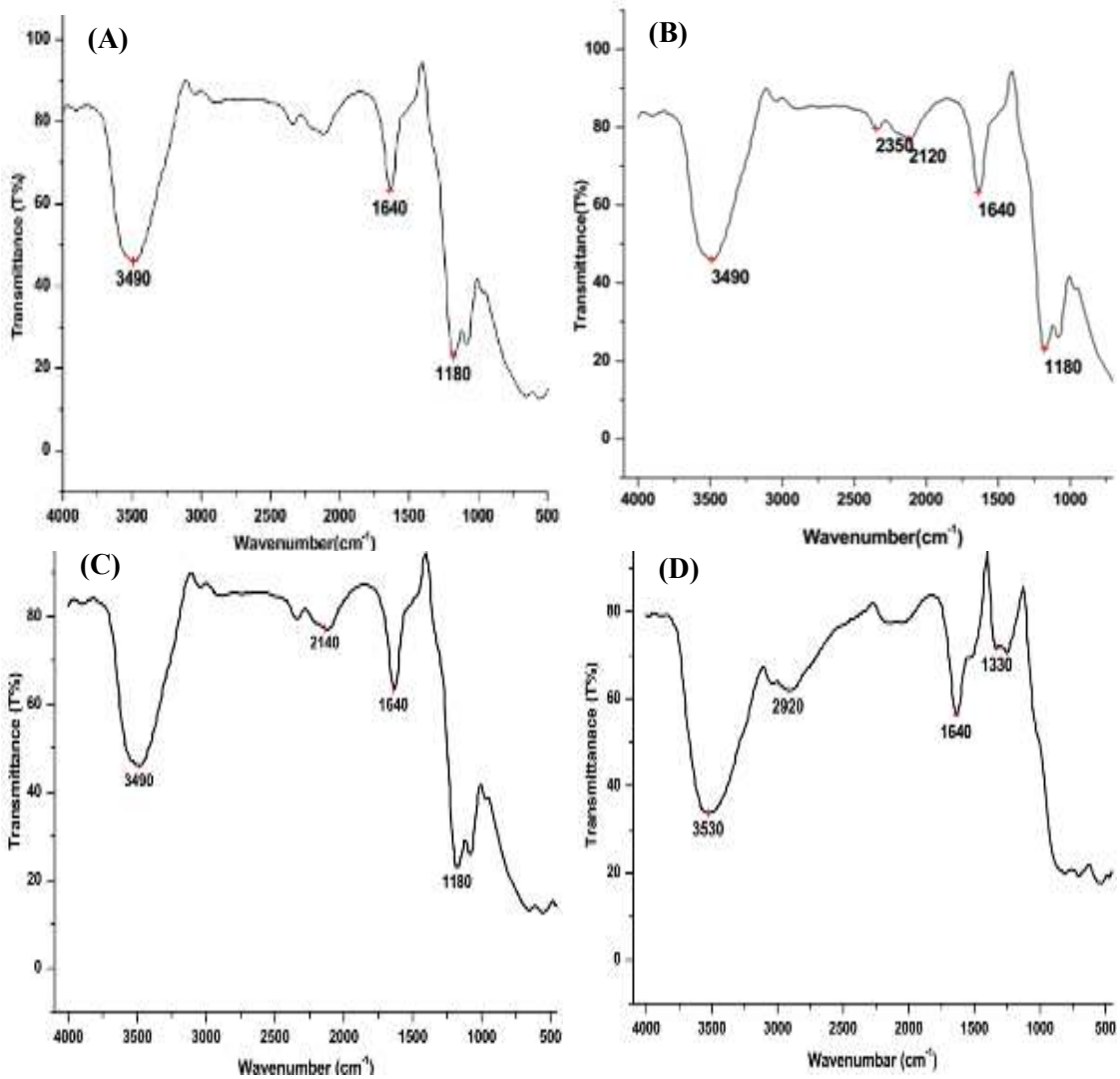

Figure 4.4: FTIR analysis of (A) $CuMn_{2RC1}$, (B) $CuMn_{2RC2}$, (C) $CuMn_{2RC3}$ and (D) $CuMn_{2RC4}$

In $CuMn_{2RC2}$ catalyst at the transmittance conditions, there are total five peaks obtained, the MnO_2 vibration mode was observed at 1640cm^{-1}, 3490cm^{-1} assigned to -OH group, 2350cm^{-1} showed Mn_2O_3 group, 1180cm^{-1} showed CuO group and 2120cm^{-1} showed C=O group. In $CuMn_{2RC3}$ catalyst at the transmittance conditions, there are total four peaks obtained, the IR band 1640cm^{-1} has showed the presence of MnO_2 group, 3490cm^{-1} showed –OH group, 1180cm^{-1} showed CuO group and 2140cm^{-1} showed CO_3^{2-} group [Guo *et al.,* 2016]. In $CuMn_{2RC4}$ catalyst at the transmittance conditions, there are total four peaks obtained, the MnO_2 vibration mode is observed at 1640cm^{-1} due to the stretching of Mn–O bond and transmission spectra at 3530cm^{-1} is assigned to –OH group. The other phases like CuO and CO_3^{2-} are present at 1330cm^{-1} and 2920cm^{-1} respectively. The spectra of impurities decrease in the following order: $CuMn_{2RC4}$ > $CuMn_{2RC3}$ > $CuMn_{2RC2}$ > $CuMn_{2RC1}$. The best result we can obtain from the FTIR analysis was that the $CuMn_{2RC1}$ catalyst has the highest purity as compared to other catalyst samples; therefore, we get the best activity results for CO oxidation. All catalysts originate from the stretching vibrations of the metal-oxygen bonds and confirm the presence of CuO and MnO_2 phases [Adánez-Rubio *et al.,* 2017].

4.2.5 Identification and quantification of elements

The XPS analysis was mainly used to understand the physical and chemical changes of catalysts by exposure of gaseous molecules under different thermal conditions examined. Although, it can be proposed that the high binding energy was preferably for CO oxidation. The prominent peak of Cu(2p) in $CuMn_{2RC1}$, $CuMn_{2RC2}$, $CuMn_{2RC3}$ and $CuMn_{2RC4}$ catalyst was deconvoluted into six peaks centered as shown in Figure 4.5. By performing peak fitting deconvolution of main Cu(2p) in all calcination catalyst was Cu(II) oxide form.

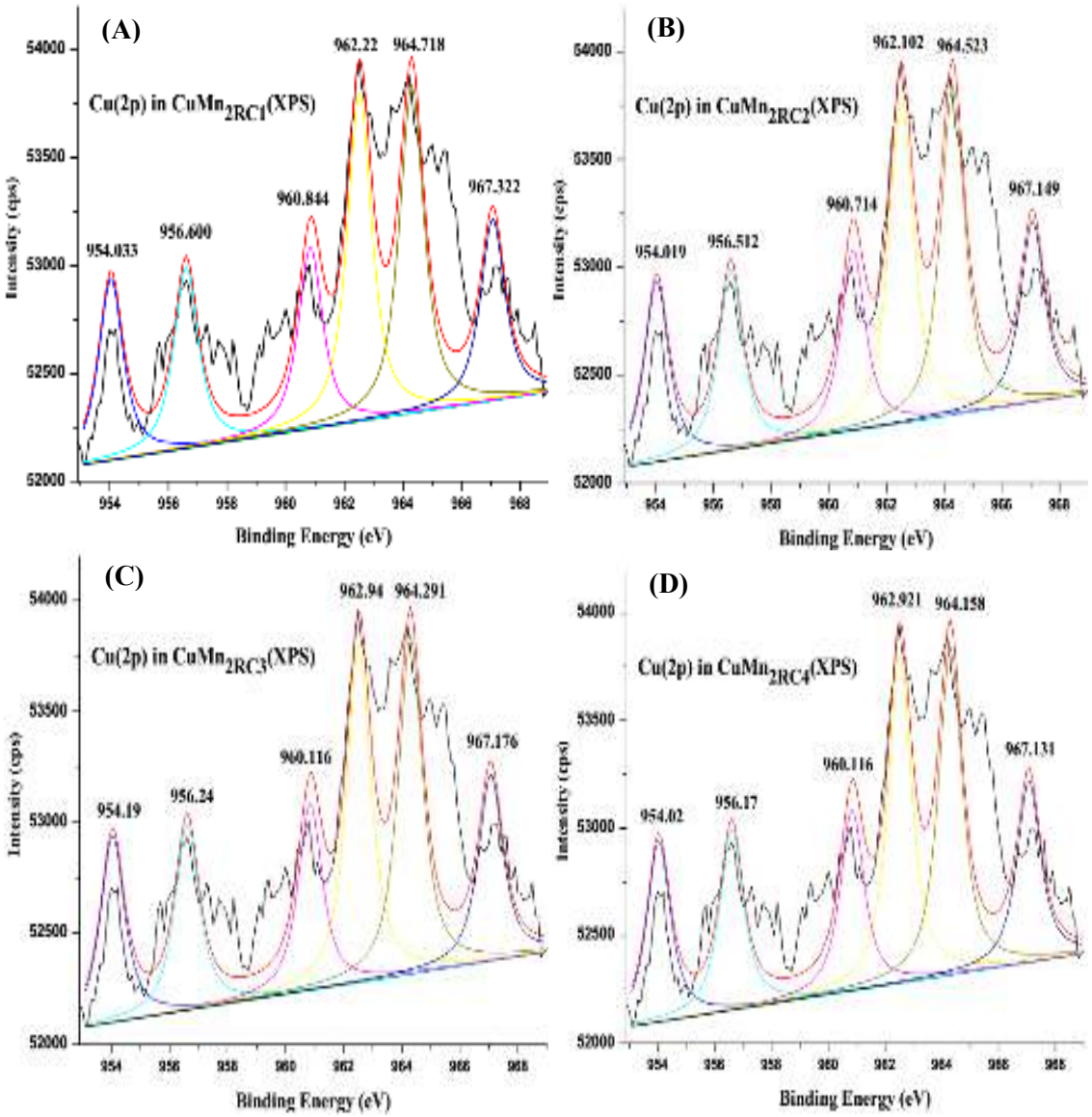

Figure 4.5: XPS analysis of Cu(2p) in (A) $CuMn_{2RC1}$, (B) $CuMn_{2RC2}$, (C) $CuMn_{2RC3}$ and (D) $CuMn_{2RC4}$

The binding energy of Cu(2p) in $CuMn_{2RC1}$ catalyst was 954.033eV, 956.600eV, 960.844eV, 962.22eV, 964.718eV and 967.322eV respectively and the highest binding energy peak of Cu(2p) in $CuMn_{2RC1}$ catalyst was obtained at 964.718eV. The binding energy of Cu(2p) in $CuMn_{2RC2}$ catalyst was 954.019eV, 956.512eV, 960.714eV, 962.102eV, 964.523 and 967.149eV respectively and the highest binding energy peak of Cu(2p) in $CuMn_{2RC2}$ catalyst was obtained at 964.523eV. The binding energy of Cu(2p) in $CuMn_{2RC3}$ catalyst was 954.19eV, 956.24eV, 960.116eV, 962.94eV, 964.291eV and

967.176eV respectively and the highest binding energy peak of Cu(2p) in $CuMn_{2RC3}$ catalyst was obtained at 964.291eV. The binding energy of Cu(2p) in $CuMn_{2RC4}$ catalyst was 954.02eV, 956.17eV, 960.116eV, 962.921eV, 964.158eV and 967.131eV respectively and the highest binding energy peak of Cu(2p) in $CuMn_{2RC4}$ catalyst was obtained at 964.158eV. The highest binding energy peak of Cu(2p) in $CuMn_{2RC1}$, $CuMn_{2RC2}$, $CuMn_{2RC3}$ and $CuMn_{2RC4}$ catalyst was 964.718eV, 964.523eV, 964.291eV and 964.158eV respectively. It was clear from Table 4.5 and Figure 4.6 that the binding energy peak of Cu(2p) in $CuMn_{2RC1}$ catalyst was highest as comparison of other catalysts. The prominent peak of Mn(2p) level in $CuMn_{2RC}$ catalyst was deconvoluted into double peak and represented in Figure 4.6. By performing peak fitting deconvolution of the main Mn(2p) in all catalyst samples, three main components including $Mn^{4+,}$ Mn^{3+} and satellite can be found. The difference between the binding energy values of Mn^{4+} and Mn^{3+} ions was small. The binding energies of Mn(2p) in $CuMn_{2RC1}$, $CuMn_{2RC2}$, $CuMn_{2RC3}$ and $CuMn_{2RC4}$ catalysts at reactive calcination conditions were (643.212eV and 655.361eV), (643.189eV and 655.349eV), (643.172 and 655.295eV) and (643.151eV and 655.285eV) respectively and it would be associated with the presence of Mn^{3+}, Mn^{4+} and satellite in all catalysts.

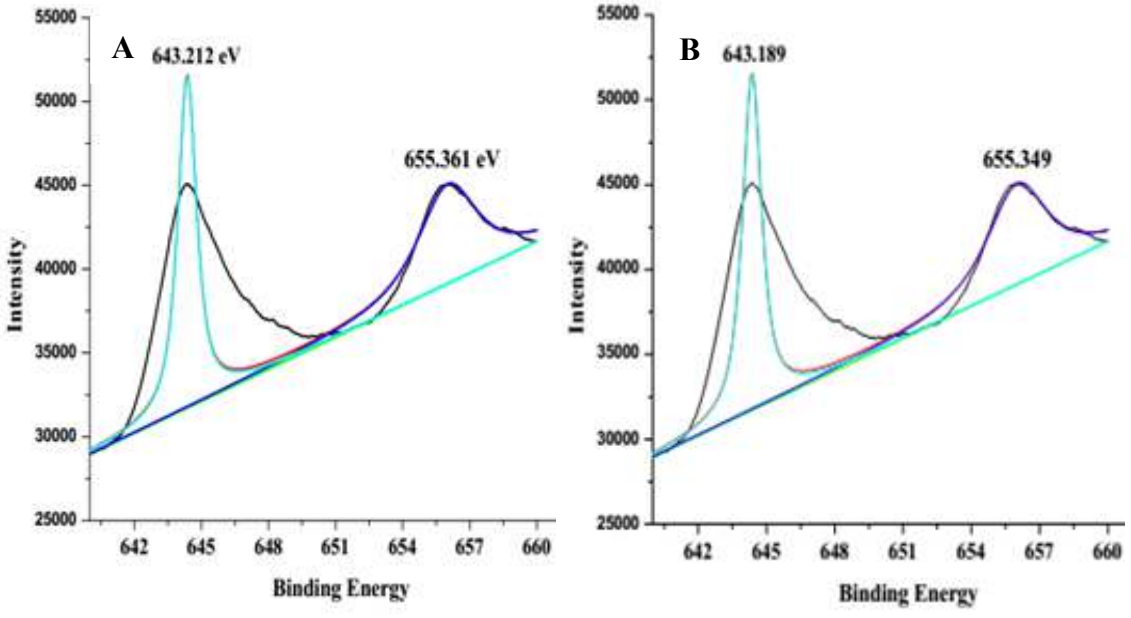

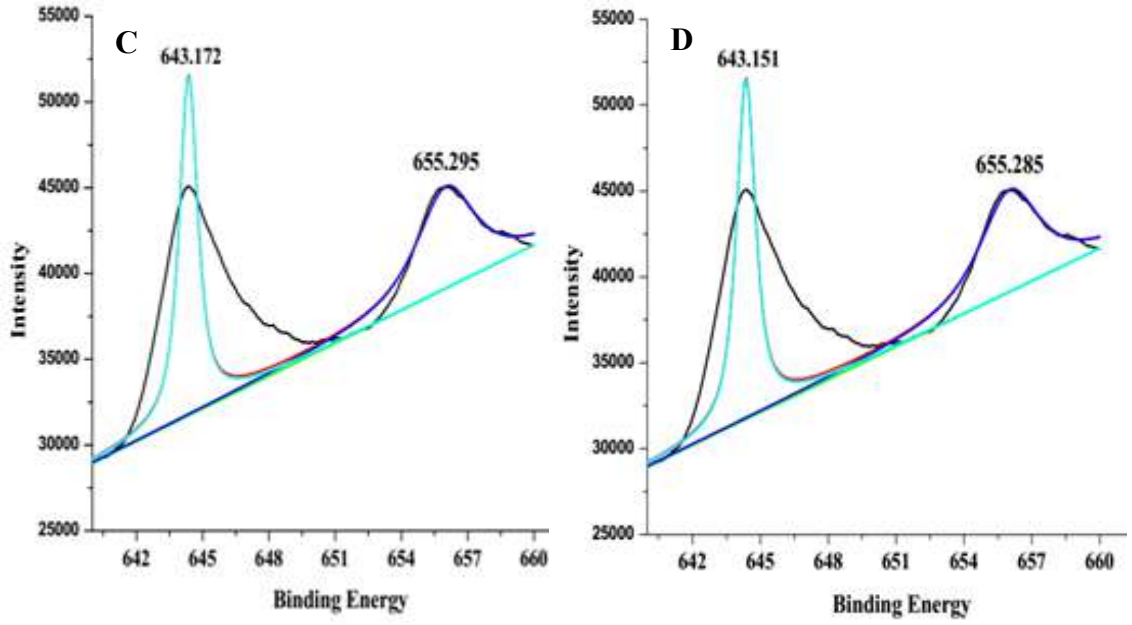

Figure 4.6: XPS analysis of Mn(2p) in (A) $CuMn_{2RC1}$, (B) $CuMn_{2RC2}$, (C) $CuMn_{2RC3}$ and (D) $CuMn_{2RC4}$

The highest binding energy peak of Mn(2p) in $CuMn_{2RC1}$, $CuMn_{2RC2}$, $CuMn_{2RC3}$ and $CuMn_{2RC4}$ catalyst was 655.361eV, 655.349eV, 655.295eV and 655.285eV respectively. Figure 4.6 shows that the broad Mn^{4+} peak presents in $CuMn_{2RC1}$ catalyst was higher than $CuMn_{2RC2}$, $CuMn_{2RC3}$ and $CuMn_{2RC4}$ catalysts.

Table 4.5: Binding energy and chemical state of $CuMn_{2RC}$ catalysts

Sample	Elements		
	Cu	**Mn**	**O**
$CuMn_{2RC1}$	Cu(II) Oxide 964.718eV	Mn_2O_3 655.361eV	C-O 529.84eV
$CuMn_{2RC2}$	Cu(II) Oxide 964.523eV	Mn_2O_3 655.349eV	C-O 529.41eV
$CuMn_{2RC3}$	Cu(II) Oxide 964.291eV	Mn_2O_3 655.295eV	C-O 529.24eV
$CuMn_{2RC4}$	Cu(II) Oxide 964.158eV	Mn_2O_3 655.285eV	C-O 529.08eV

It was clear from Table 4.5 and Figure 4.6 that the binding energy of Mn(2p) present in $CuMn_{2RC1}$ catalyst was highest as compared to the other catalyst samples. In the present study, the oxygen with the binding energy of 529.58eV was the main form and could be assigned to the chemisorbed oxygen (Oa). The presence of lattice oxygen was very small in $CuMn_{2RC1}$ catalyst. The binding energy of O(1s) in $CuMn_{2RC1}$, $CuMn_{2RC2}$, $CuMn_{2RC3}$ and $CuMn_{2RC4}$ catalyst was 529.84eV, 529.41eV, 529.24eV and 529.08eV respectively. The chemical state of Cu, Mn and O present in $CuMn_{2RC}$ catalyst was Cu(II) Oxide, Mn_2O_3 and C-O form (Table 4.5) respectively. One of noticeable fact was that the amount of oxygen presents in reactive calcined prepared $CuMn_{2RC1}$ catalyst was least as compared to $CuMn_{2RC2}$, $CuMn_{2RC3}$ and $CuMn_{2RC4}$ catalysts, due to an absence of lattice oxygen which creates oxygen vacancies for the CO oxidation. The content order of $O_a/(O_a+O_l)$ ratio was shown as following: $CuMn_{2RC1}$> $CuMn_{2RC2}$> $CuMn_{2RC3}$> $CuMn_{2RC4}$. The presence of higher oxidation state phases could be the result of a greater degree of surface interface between the easily oxidisable manganese phase and highly reducible copper phase. The high amount of surface chemisorbed oxygen (most active oxygen) was more preferable for enhancing the catalytic activity for CO oxidation.

4.2.6 Surface area measurement

The N_2 adsorption-desorption isotherms and Pore size distributions curves of $CuMn_{2RC}$ catalysts prepared by the co-precipitation method with a novel route of reactive calcination are shown in Figure 4.7(A) and (B) respectively. BET surface area of the $CuMn_{2RC}$ catalysts is given in Table 4.6. Clearly, the textural property of $CuMn_{2RC1}$ catalyst was better to those of $CuMn_{2RC2}$, $CuMn_{2RC3}$ and $CuMn_{2RC4}$ catalyst. It can be visualized from the Table 4.6 that the BET surface area and pore volume of $CuMn_{2RC1}$ catalyst were much higher than the other catalyst samples. The isotherm gave valuable information on the mesopores structure through its hysteresis loop.

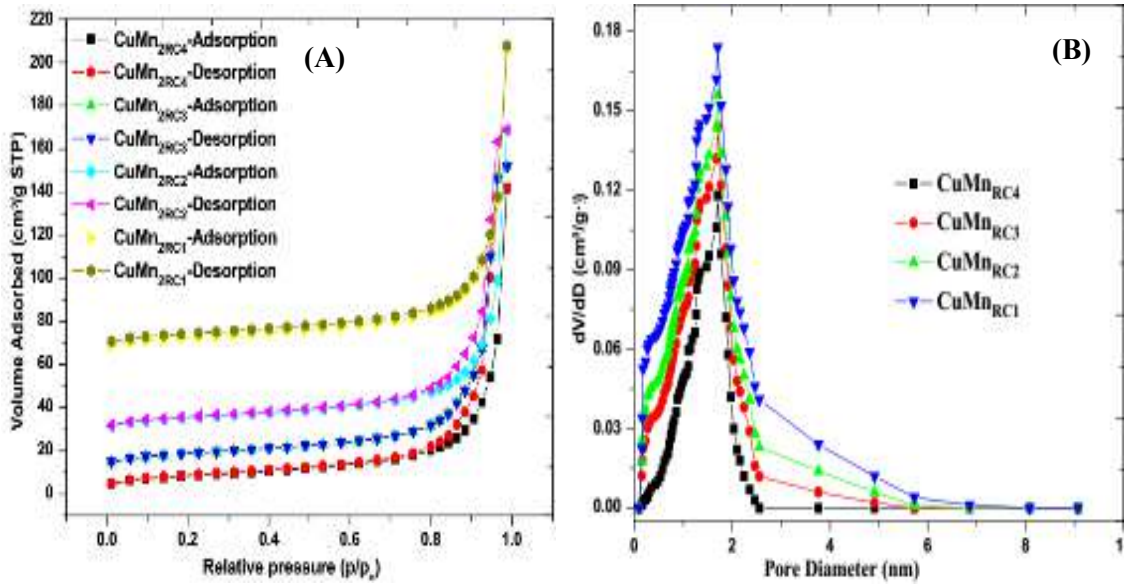

Figure 4.7: Textural properties (A) N_2 adsorption-desorption isotherms and (B) Pore size distributions curves

The prepared catalysts exhibited hysteresis loop, which indicated that the pores were exhibiting geometries of mesopores. The existence of hysteresis loop at a relative pressure (P/P_0) of 0.8–1.0 indicates that the porosity arising from the non-crystalline intra-aggregate voids and spaces formed by inter-particle contacts. Figure 4.7(B) shows that the pore size distributions (PSDs) as calculated by the Barrett–Joyner–Halendar (BJH) method from the desorption branch of nitrogen isotherms.

Table 4.6: Textural property of $CuMn_{2RC}$ catalysts

Catalyst	**Surface Area (m^2/g)**	**Pore Volume (cm^3/g)**	**Ave. Pore Size (Å)**
$CuMn_{2RC1}$	118.24	0.627	49.45
$CuMn_{2RC2}$	106.85	0.572	56.40
$CuMn_{2RC3}$	95.21	0.519	63.65
$CuMn_{2RC4}$	88.25	0.468	70.65

The porous textural parameters, such as specific surface area (S_{BET}) and pore volume (V_{total}) are also listed in the Table 4.6. The surface area of $CuMn_{2RC1}$, $CuMn_{2RC2}$, $CuMn_{2RC3}$ and $CuMn_{2RC4}$ catalyst was 118.24, 106.85, 95.21 and 88.25m^2/g respectively. Specific surface area and total pore volume were two significant factors which can affect the catalytic activity for CO oxidation. The catalyst surface areas of similar magnitude regardless of the preparation atmosphere; however, there was a general increase in surface area as a result of choosing suitable precursors. The average pore diameter was increased with the increasing of calcination temperature because a high-temperature treatment led to particle sintering accompanied with a loss in the active area. A large number of more pores present in a catalyst surface mean a higher number of CO molecules were captures on their surface; therefore, it has to shows the superior catalytic activity. The specific surface area was measured by BET analysis and it was also following the SEM and XRD results.

4.3 Catalyst performance and activity measurement

Activity test of the catalyst was carried out to evaluate the efficiency of $CuMn_2$ catalysts formed under different calcination conditions as a function of temperature. Activity was increased with the increasing of temperature from room temperature to certain high temperature for full conversion of CO. The light-off characteristics were used to evaluate the activity of resulting catalysts with the increasing of temperature. The characteristic temperature T_{10}, T_{50} and T_{100} corresponds to the initiation of oxidation, 50% conversion and full conversion of CO respectively. The improved activity of the catalysts can be ascribed to the unique structural, textural characteristics and the smallest crystallite size.

4.3.1 Activity of catalysts produced under stagnant air calcination

Activity of $CuMn_{2SA}$ catalysts produced under stagnant air calcination of precursors for CO oxidation was measured in laboratory. The $CuMn_{2SA}$ catalyst was extremely influenced by a combination of factors including preparation conditions, drying temperature, calcination conditions and the presence of Cu^{2+}, Mn^{2+} and O on the surface of catalyst. The calcination of $CuMn_2$ precursor was done in a muffle furnace in stagnant air. The catalytic activity tests were carried out to evaluate the activity of resulting catalysts as a function of temperature. The activity plot and the light off characteristics are shown in Figure 4.8 and Table 4.7 respectively. A clean surface was exposed by a mixture of CO and air quickly becomes enclosed with CO since it requires a single vacant adsorption site. The interaction between various chemical compounds (Cu-Nitrate or Cu-Acetate and Mn-Nitrate or Mn-Acetate) with the precipitation agent $KMnO_4$ the formation of a highly disordered mixed metal oxide was the cause of high catalytic activity for CO oxidation.

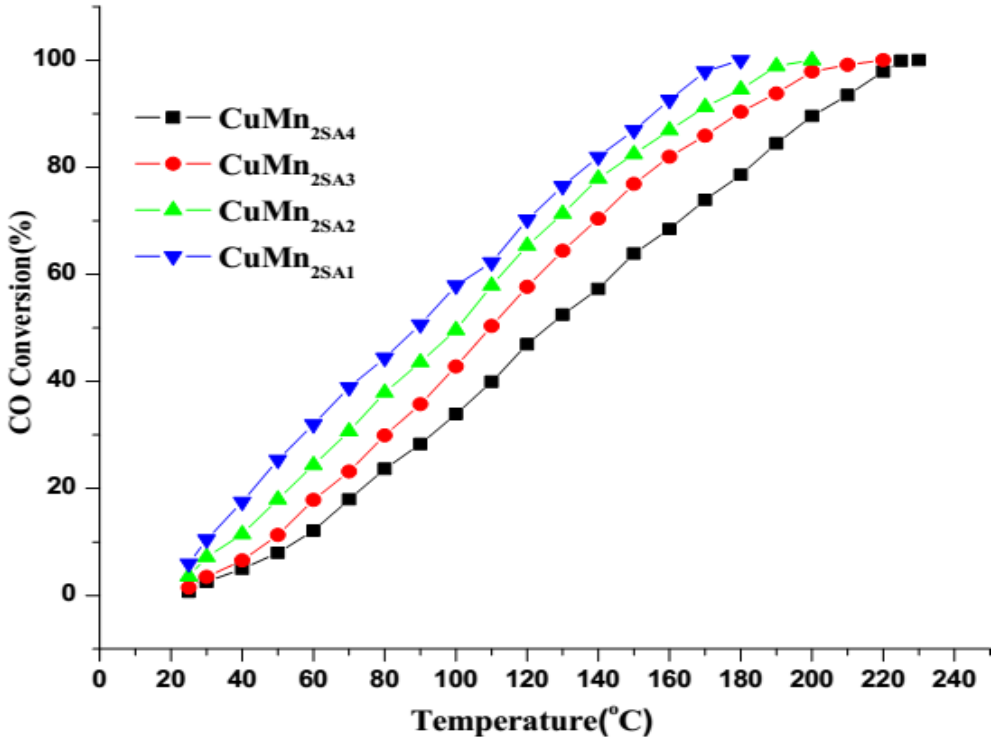

Figure 4.8: Catalytic activity of various $CuMn_{2SA}$ catalysts for CO oxidation

It was evident from the Table 4.7 and Figure 4.8 that the oxidation of CO has initiated near the room temperature ~25°C and 50% conversion of CO was occurred at 90ºC over the $CuMn_{2SA1}$ catalyst, which was less by 10ºC, 20ºC and 30ºC over than that of $CuMn_{2SA2}$, $CuMn_{2SA3}$ and $CuMn_{2SA4}$ catalyst respectively. The total oxidation temperature of CO was 180°C for $CuMn_{2SA1}$, which was less by 20°C, 30°C and 50°C over than that of $CuMn_{2SA2}$, $CuMn_{2SA3}$ and $CuMn_{2SA4}$ catalysts respectively.

Table 4.7: Light-off characteristics of $CuMn_{2SA}$ catalysts

Catalyst	T_{10}	T_{50}	T_{100}
$CuMn_{2SA1}$	25ºC	90ºC	180ºC
$CuMn_{2SA2}$	25ºC	100ºC	200ºC
$CuMn_{2SA3}$	25ºC	110ºC	210ºC
$CuMn_{2SA4}$	25ºC	120ºC	230ºC

The $CuMn_{2SA1}$ catalyst has shown the excellent catalytic activity for CO oxidation as compared to the other catalysts. The activity order of each catalyst for total oxidation of CO was in accordance with their characterization. The order of activity of different types of $CuMn_{2SA}$ catalysts for CO oxidation was as follows: $CuMn_{2SA1}$> $CuMn_{2SA2}$> $CuMn_{2SA3}$> $CuMn_{2SA4}$. Using the $KMnO_4$ precipitant, the catalysts prepared with a combination of $\{Mn(Ac)_2 + Cu(NO_3)_2\}$ as the precursors were considerably more effective than the other catalyst samples. An activity of the multiphase catalysts CuO and MnO_2 were several times superior to those of single phase oxides CuMnOx catalyst, especially in the lower temperature range. The coordination between Mn-oxide and Cu-oxide in an appropriate proportion into the CuMnOx catalyst, was an improving their performance for CO oxidation.

4.3.2 Activity of catalysts produced under flowing air calcination

The activity of the catalyst produced in the flowing air calcination of the precursors was measured with the increasing of temperature under steady state conditions. The results are shown in the Figure 4.9. The oxidation of CO initiated at room temperature ~25°C over all the catalysts and 50% conversion of CO over the $CuMn_{2FA1}$ catalyst was found at 70°C, which was less by 10°C, 30°C and 50°C over than that of $CuMn_{2FA2}$, $CuMn_{2FA3}$ and $CuMn_{2FA4}$ catalysts respectively. The total oxidation temperature of CO was 120ºC for $CuMn_{2FA1}$ catalyst, which was less by 30°C, 55°C and 70°C over than that of $CuMn_{2FA2}$, $CuMn_{2FA3}$ and $CuMn_{2FA4}$ catalysts respectively. As compared to calcination in stagnant air, the flowing air created more active catalysts for CO oxidation at a lower temperature. The order of activity of catalysts calcined under flowing air (FAC) was higher than that of stagnant air (SAC) i.e.: FAC > SAC.

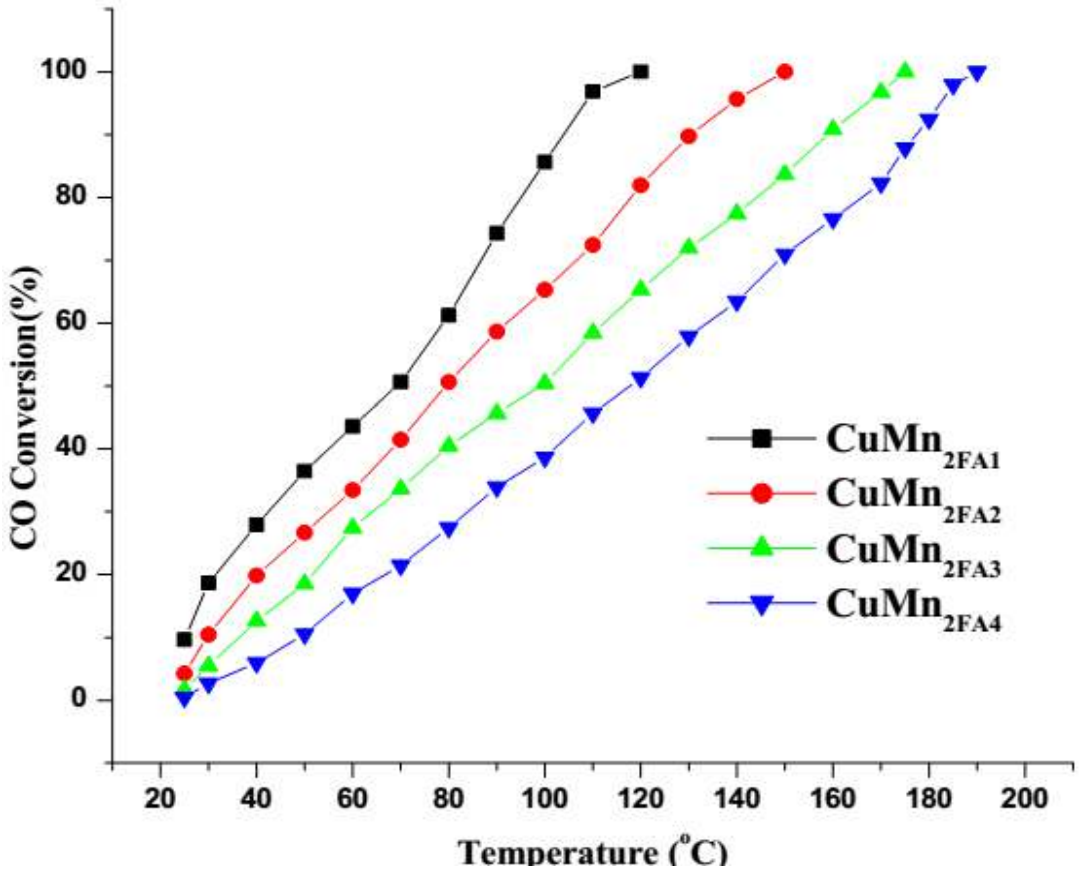

Figure 4.9: Catalytic activity of various $CuMn_{2FA}$ catalysts for CO oxidation

The order of activity of different types of Cu_1Mn_2 catalysts for CO oxidation was as follows: $CuMn_{2FA1}$> $CuMn_{2FA2}$> $CuMn_{2FA3}$> $CuMn_{2FA4}$. Thus, the $CuMn_{2FA1}$ catalyst has exhibited the highest activity for CO oxidation. Keeping the same precipitant while changing the precursor caused a high influence on the CO oxidation activity.

Table 4.8: Light-off characteristics of $CuMn_{2FA}$ catalysts

Catalyst	**T_{10}**	**T_{50}**	**T_{100}**
$CuMn_{2FA1}$	25ºC	70ºC	120ºC
$CuMn_{2FA2}$	25ºC	80ºC	150ºC
$CuMn_{2FA3}$	25ºC	100ºC	175ºC
$CuMn_{2FA4}$	25ºC	120ºC	190ºC

The catalyst prepared by a combination of {$Mn(Ac)_2$ + $Cu(NO_3)_2$} as precursors were significantly more active than the catalysts obtained by other combinations. A suitable combination of various chemical compounds present in the precursor resulted in the most efficient CO oxidation catalyst.

4.3.3 Activity of catalysts produced under reactive calcination

The RC process minimized a process step by converting two steps processes into single step process in a reactive CO-air mixture at a 300^{o}C. It also produced $CuMn_{2RC}$ catalysts with better performance for CO oxidation (Figure 4.10). The oxidation of CO over $CuMn_{2RC}$ catalysts produced by RC method initiated at room temperature ~25°C. The 50% conversion of CO over the $CuMn_{2RC1}$ catalyst was 45°C, which was less by 10°C, 25°C and 40°C over than that of $CuMn_{2RC2}$, $CuMn_{2RC3}$ and $CuMn_{2RC4}$ catalysts respectively.

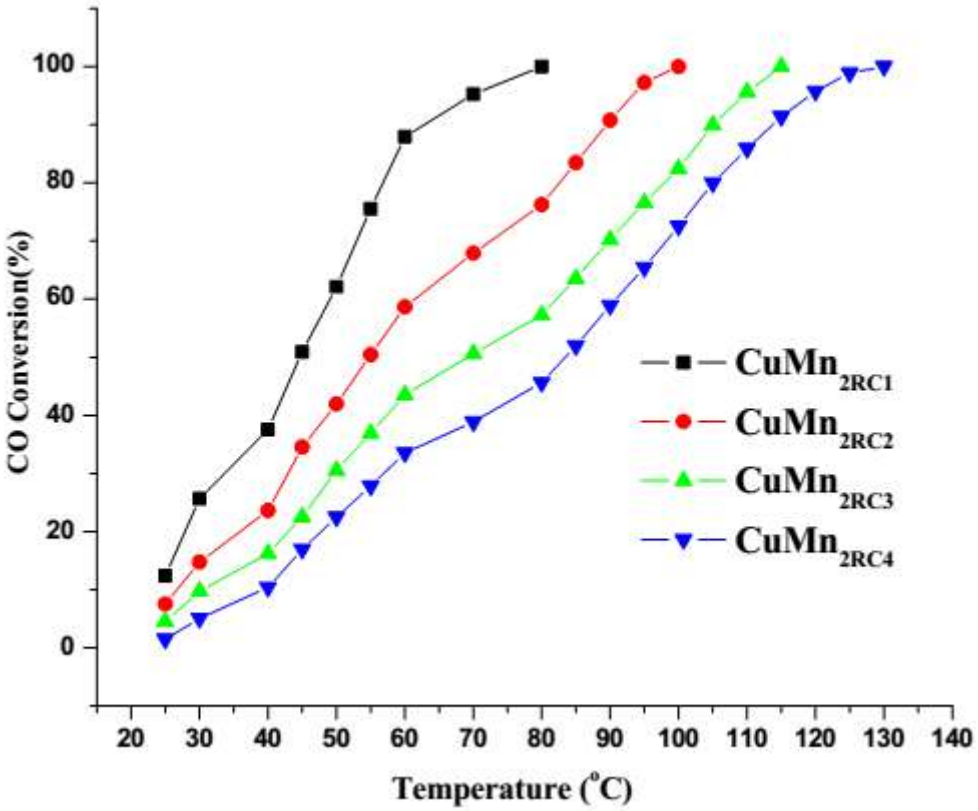

Figure 4.10: Catalytic activity of various $CuMn_{2RC}$ catalysts for CO oxidation

The total oxidation temperature of CO was 80ºC for $CuMn_{2RC1}$ catalyst, which was less by 20°C, 35°C and 50°C over than that of $CuMn_{2RC2}$, $CuMn_{2RC3}$ and $CuMn_{2RC4}$ respectively. It was clear from the light off characteristics Table 4.9 that the $CuMn_{2RC1}$ has shown the best catalytic activity for CO oxidation than the $CuMn_{2RC2}$, $CuMn_{2RC3}$ and $CuMn_{2RC4}$ catalysts.

Table 4.9: Light-off characteristics of $CuMn_{2RC}$ catalysts

Catalyst	**T_{10}**	**T_{50}**	**T_{100}**
$CuMn_{2RC1}$	25ºC	45ºC	80ºC
$CuMn_{2RC2}$	25ºC	55ºC	100ºC
$CuMn_{2RC3}$	25ºC	70ºC	115ºC
$CuMn_{2RC4}$	25ºC	85ºC	130ºC

The order of activity of different types of Cu_1Mn_{2RC} catalysts for CO oxidation was as follows: $CuMn_{2RC1} > CuMn_{2RC2} > CuMn_{2RC3} > CuMn_{2RC4}$. As compared to calcination in stagnant air and flowing air the reactive calcination produced more active catalysts for CO oxidation at a relatively lower temperature.

4.3.4 Comparison of reactive calcination with traditional calcination

The RC route was the most appropriated calcination strategy for the production of highly active Cu_1Mn_2 catalyst for CO oxidation. A comparative study of CO oxidation over the ($CuMn_{2SA1}$, $CuMn_{2FA1}$ and $CuMn_{2RC1}$) catalysts formed under the various calcination conditions was shown in the Figure 4.11. The calcination strategies have a strong effect on the activity of resulting catalyst. The oxidation of CO was initiated at 25°C overall all the catalyst samples and 50% conversion of CO over the $CuMn_{2RC1}$ catalyst was 45°C, which was less by 25°C and 45°C over than that of $CuMn_{2FA1}$ and $CuMn_{2SA1}$ catalysts respectively.

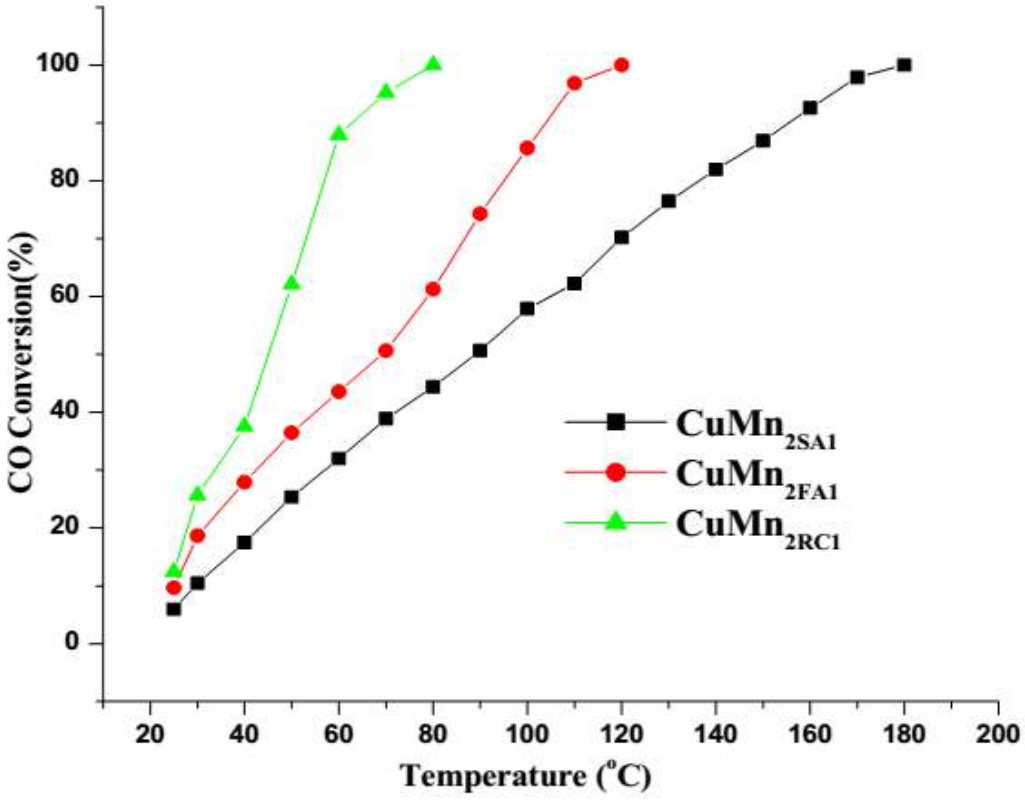

Figure 4.11: Activity test of $CuMn_2$ catalysts under various calcination conditions

The complete conversion temperature of CO was 80ºC for $CuMn_{2RC1}$ catalyst, which was less by 40°C and 100°C over than that of $CuMn_{2SA1}$ and $CuMn_{2FA1}$ catalysts respectively. The activity order of CO oxidation in the decreasing sequence was in accordance with their characterization by SEM-EDX, BET, XRD, XPS and FTIR as follows: $CuMn_{2RC1}$> $CuMn_{2FA1}$> $CuMn_{2SA1}$. The better catalytic activity of reactive calcination can be ascribed to the unique structural and textural characteristics as the least crystallites of $CuMn_{2RC1}$. The highly dispersed and high specific surface area which could expose more active sites for the catalytic oxidation and relatively open-textured pores which will favor for the adsorption of reactants and desorption of products and thus facilitate the oxidation process.

Table 4.10: Light-off characteristics of Cu_1Mn_2 catalysts

Catalyst	**T_{10}**	**T_{50}**	**T_{100}**
$CuMn_{2SA1}$	25ºC	90ºC	180ºC
$CuMn_{2FA1}$	25ºC	70ºC	120ºC
$CuMn_{2RC1}$	25ºC	45ºC	80ºC

The presence of partially reduced phase provides an oxygen deficient defective structure which creates a high density of active sites as a result of reactive calcination, consequently $CuMn_{2RC1}$ turn into the most active catalyst. The highest activity of $CuMn_{2RC1}$ catalyst was associated with the creation of smallest crystallites authenticated by XRD observation. Using the Cu_1Mn_2 catalyst, the precursors have changed the highly influenced activity of resulting catalysts. Finally, it was found that the various precursors could lead to different crystalline phase formation of the Cu_1Mn_2 catalysts. The crystalline phases of dried samples prepared by various types of precursors were all

distinct despite being synthesized with the same catalyst. The combination of precipitant and precursor in the precipitation process plays an important role in the production of highly active catalysts.

4.4 Concluding Remarks

The CuMnOx catalysts have been synthesized using $\{Mn(Ac)_2 + Cu(NO_3)_2\}$, $\{Mn(Ac)_2 + Cu(Ac)_2\}$, $\{Mn(NO_3)_2 + Cu(NO_3)_2\}$, $\{Mn(NO_3)_2 + Cu(AC)_2\}$ as precursor precipitated by $KMnO_4$ solution and their catalytic activity for CO oxidation has been evaluated. The various precursors have a significant influence on the structural properties and catalytic activity of $CuMnO_x$ catalyst for CO oxidation. The catalyst prepared by $\{Mn(Ac)_2 + Cu(NO_3)_2\}$ as a precursors exhibits the best catalytic activity for CO oxidation due to the high oxygen mobility. Maintaining the same precipitant, while changing the precursor causes a change in the density of active sites which influence the CO oxidation. The calcination strategies of the precursor have a great influence on the activity of resulting catalysts. The calcination order with respect to the performance of catalyst for CO oxidation is as follows: reactive calcination> flowing air> stagnant air. The RC route is the most appropriated calcination strategy for the production of highly active $CuMn_{2RC1}$ catalyst.